Nano Research

Open Access

Research Article

Polymorphic signal responses of phase-change quantum dot string upon stochastic resonance

Qin Wan[1], Fei Zeng[1,2] ✉, Ziao Lu[1], Junwei Yu[1], and Feng Pan[1]

[1] Key Laboratory of Advanced Materials (MOE), School of Materials Science and Engineering, Tsinghua University, Beijing 100084, China
[2] Center for Brain Inspired Computing Research (CBICR), Tsinghua University, Beijing 100084, China

Cite this article: *Nano Research*, **2025**, *18*, 94907088. https://doi.org/10.26599/NR.2025.94907088

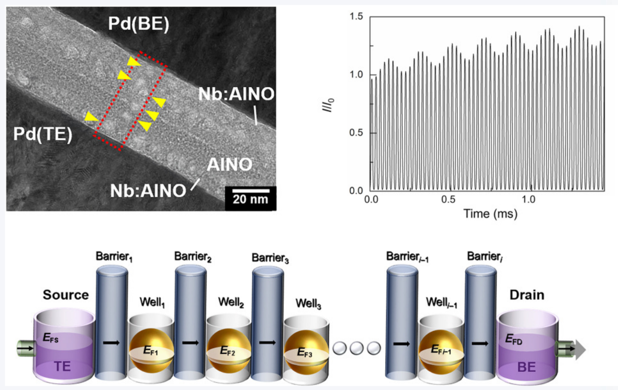

ABSTRACT: We successfully constructed phase-change quantum dots string (PCQDS) systems and studied their signal responses. The PCQDS actually is a cascaded structure consisted of several stochastic resonance (SR) two-state systems, in which inherent non-linearity, i.e., phase-change of quantum dots (QDs), plays elementary and important roles to modulate signal output. We established an SR model to simulate signal responses depending on stimulation history. We know that some QDs will oscillate with input forcing frequency, while certain QDs will oscillate in their own frequency triggered by phase transition. These two effects cooperate to generate polymorphic response patterns, including action potential patterns exhibited by envelope of spike peak values. An interesting and important simulation is that we replicate the memory effect in Nb-doped AlNO, i.e., a QDs dispersed system. The result indicates that memory can occur in a system only constructed by volatile elementary units, implying memory existing in network. Long-term plasticity and spike-rate dependent plasticity can also be realized by using frequency and phase modulation. Our study provides a new scope to study signal handling and memory effect in quantum system.

KEYWORDS: quantum-dot string, phase-change, inherent nonlinearity, signal modulation, niobium oxide, stochastic resonance

1 Introduction

Signal processing in quantum system has attracted extensive interest for several decades because it is assumed to be low power consumption and intelligent as well as that in neural network. Particularly, our interest is to study a cascaded quantum system by using stochastic resonance (SR) theory and methods. In one aspect, SR handles noise to optimize weak signal processing in nonlinear threshold systems [1]. In the other aspect, the cascaded quantum system is akin to the cascaded neurons in neural network. The SR has various implications in neuroscience under both inherent noise and external noise to enhance neuronal communication [2–7]. The SR has enhanced visual receptor [8], cochlear implants and hearing [9, 10], mechanoreceptor [11–14], muscle receptor [15], cardiac regulation [16], muscle motor units [17–19], precision of finger force [14], and vibratory tactile sensation [20]. The essence of these phenomena is that in a neural circuit, the first neuron linked to the sensor intercepts signals and disseminates them along the neuronal string through the SR effect across adjacent synaptic junctions, resulting in amplified oscillatory spike pulses [21]. Therefore, we propose a cascaded quantum system named as phase-change quantum dot string (PCQDS) and studied its signal responses to compare with those of cascaded neuron system.

The phase-change quantum dot (PCQD) is the NbO quantum dot (QD) firstly fabricated by using a self-assembly method in Nb-doped AlNO layers [22, 23]. We constructed lately a single PCQD system and found that it can fire two types of quantized and periodical signals depending on the methods modulating tunneling processes [24]. The single PCQD system is a double-barriers quantum system corresponding to a pair of coupled SR two-state structures [25, 26]. The phase-change of NbO QD is the inherent nonlinearity to modify the dimension of barriers and well depending on the signal strength and history. The PCQDS in this study connects several PCQDs in series so that it can be treated as

Received: July 14, 2024; **Revised:** October 11, 2024
Accepted: October 21, 2024

✉Address correspondence to zengfei@mail.tsinghua.edu.cn

the cascaded SR two-state structures. Besides, because neuroscience usually stimulates neural system by using highly structured pulse sequences, including peripheral nerve stimulators, spinal cord stimulators, and deep brain stimulators [27–30], we adopted the square pulse embedded by the structured noise and abandoned the broadband noise usually used in physics [1, 31–36].

We studied the signal responses of PCQDS according to our cascaded SR model and found a set of interesting results. Our model revealed that the PCQDS not only synchronizes with external inputs but also embeds the distinctive oscillation of certain neurons (QDs) into those signal responses. Upon simulation, we replicated intricate learning protocols including short-term plasticity (STP), long-term plasticity (LTP), spike-rate dependent plasticity (SRDP) [37], and neural spike firing.

2 Results and discussion

The PCQDS was obtained after a set of self-assemble processes. The functional multilayer AlNO:Nb/AlNO/AlNO:Nb was firstly prepared between two Pd electrode layers by co-sputtering method. Subsequently, we manipulated approximately 0.5 V voltage sweep on the Pd/AlNO:Nb/ AlNO/AlNO:Nb/Pd device to fulfill an electrical forming process, after which the NbO QDs formed in the Nb-doped AlNO layers. Those QDs distribute within a distance of 16 nm near bottom electrode (BE) and that of 8 nm near top electrode (TE). We finally stimulated the device by using the square pulse with an amplitude of 2 V, a width of 10 µs, and a frequency of 30,000 Hz. The pulse responses became stable when the pulse number exceeded 10,000. At this time, the two PCQD bands near electrodes were broadened slightly and a PCQDS clearly crossed over the multilayers. We have also considered the influence of inject energies on the QDs size. We have found that when the bias voltage was very low, the residual Nb atoms could not obtain enough energy to migrate cross the undoped layer. At this time, the QDs could not form in the middle AlNO layer. When the bias voltage was very high, the long-distance migration would occur to result in coarsening between the doped and undoped layers.

Figures 1(a)–1(e) illustrate the resembles in structure and signal responses between a neuron string and a PCQDS. The SR in the cascaded neuron systems is presented in Fig. 1(b) [21]. The first neurons receiving stimuli from sensors are "pacemakers" (Fig. 1(b), yellow neuron). They usually are autonomous nerve cells in biological tissues, such as cardiac and arterial tissue [38, 39], to transfer their oscillatory rhythm to neighboring cells, and to initiate SR to conduct information through the entire neural circuit and regulate the physiological activity of the entire tissue. Albert et al. validated the cardiac contractions triggered by periodic pulse trains with appropriate frequency, amplitude, and pulse duration in isolated mouse hearts, as shown in Fig. 1(c) [16]. The response pattern indicates that the neurons can follow the input frequency firstly. The envelope of individual spike peak (red line) demonstrates that the strength alternatively increases with the input number indicating long-term potentiation, which is a result of particular nonlinear coupling in the cascade neural string during different stages.

In addition, the envelope presents cyclical oscillation features. The response pattern is the modulated output manipulated by the certain actions from the cascaded neurons. The spike envelope can exhibit more waveforms to convey more information through this SR system. For the instance in Fig. 1(c), the physical meaning of the

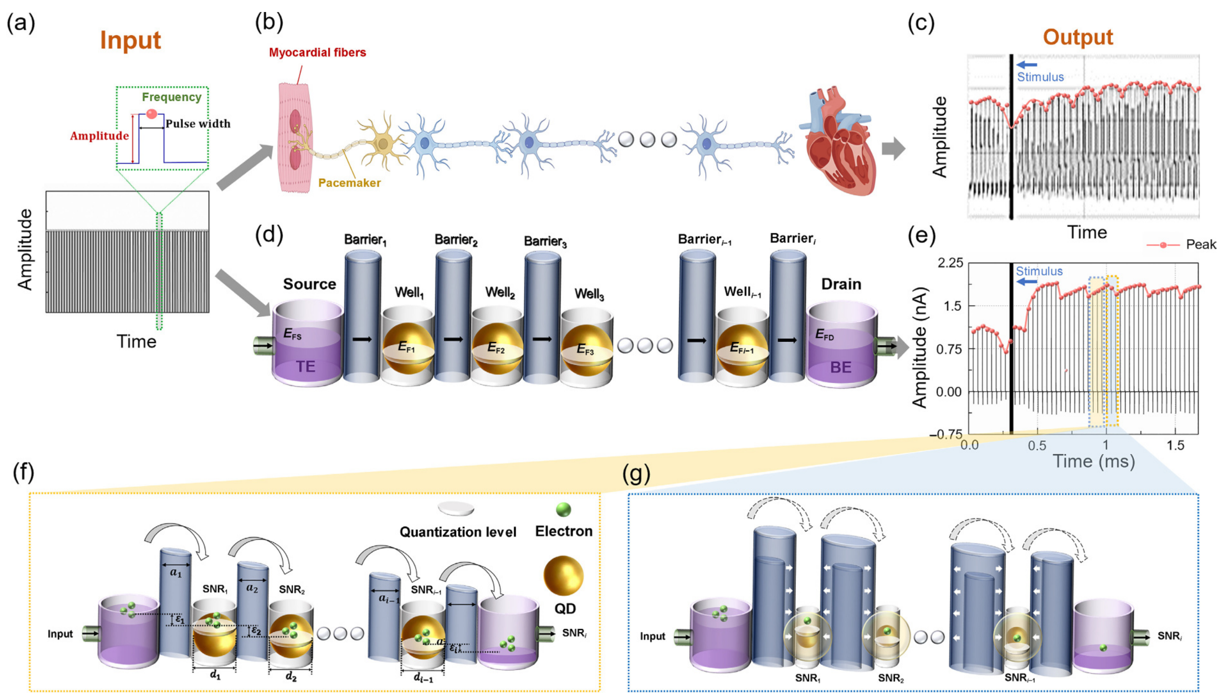

Figure 1 Comparison between the signal responses of the cascaded neurons and the PCQDS via SR. (a) Input is a structured pulse sequence, i.e., a square pulse series used for the two cascaded systems. (b) Schematics of the cascaded neurons according to the experiments testing mouse heart contraction [16]. Black arrow indicates the signal direction. (c) Periodic heart contractions triggered by electrical stimulation are amplified and modulated by SR. The envelope (red line) of the spike series exhibits clear cyclical oscillation. The input series is scaled by a frequency of 7 Hz, an amplitude of 3 V, and a pulse width of 4 ms. (d) Schematics of the cascaded potential barriers and wells in PCQDS. (e) The SR rhythm of PCQDS. The input series is scaled by a frequency of 30,000 Hz, an amplitude of 2 V, and a pulse width of 10 µs. Possible explanations of cycled zones in (e) are illustrated in (f) and (g), respectively. (f) Amorphous-crystalline transition occurs for certain PCQD during tunneling process. (g) Crystalline-amorphous transition occurs for certain PCQD during tunneling process.

cosine envelope represents the contractile behavior of an isolated rat heart. The spike signal represented by the black line in Fig. 1(c) is an acquired signal composed of electromyography (EMG) and bioimpedance. Since the amplitude of the myoelectric component is much lower than the amplitude of the bioimpedance, it is difficult to identify in this diagram. If we extract and connect the peaks of these spikes, we get the separated signal component, which is the envelope. It mainly represents the myoelectric component. The time scale of device oscillation is in the order of μs (Fig. 1(e)), which is faster than that of biological neurons (Fig. 1(c)). If the pulse width is reduced but the pulse amplitude is unchanged, the time scale should be enlarged because the injected energy per pulse decreases. The oscillatory behaviors in this manuscript will not maintain. This will be our interest in the next study.

The PCQDS connects several SR two-state systems in series, as shown in Fig. 1(d). An individual two-state system corresponds to a neuron shown in Fig. 1(b). The responses pattern in Fig. 1(e) also shows that the system follows input frequency in one aspect and the envelope of output (red line) oscillates as well as that in Fig. 1(c) in the other aspect. We extract output signal parameters from Figs. 1(c) and 1(e) and list them in Table 1 to compare the similarities and differences in the amplitude and frequency between the neuron string and the PCQDS. Consequently, the PCQDS can play the same role in modulating spike output as the cascaded neurons. The possible reasons for the oscillation in Fig. 1(e) come from the amorphous-crystalline transition of certain QDs, as illustrated in Figs. 1(f) and 1(g). When the amorphous phase transforms to the crystalline phase, the effective potential barriers would decrease and then the overall conduction increases to lead to the ascending of spike peaks, as shown in Fig. 1(f). On the contrary, the crystalline to amorphous transition leads to the descending of spike peaks, as shown in Fig. 1(g). Either the ascending or the descending may be induced by the individual QD action or the cooperation of several QDs. Because it is difficult to detect the individual dynamical behavior of either the neuron or the QD by using the present microscopical techniques, the study of PCQDS depending on appropriate structure and dynamical model will become effective and comprehensible.

We established an SR model for PCQDS so that we can correlate those particular responding patterns to the dynamic actions of potential barriers and wells [40]. A QD embedded structure is actually a double barrier system treated as two connected two-state systems in series. Tunnelling through the double barrier needs to enhance the Fermi level of the source comparable to the quantized level in the potential well or on the QD. This energy disparity is designated as asymmetric energy ε_i, where i is the i^{th} two-state system. However, if $i = 1$, there is not QD so that the system is a single barrier system and ε_1 is the energy disparity between the top TE and the BE. $i > 2$ corresponds to i barriers and $i - 1$ QDs (or potential well). The signal-to-noise ratio (SNR) of the current signal generated after tunneling i barriers is termed SNR_i. Owing to the reversible "crystalline ↔ amorphous" phase transition of QD [24], the diameter (d_{i-1}) of QD oscillates and conducts to the neighbored barrier width (a_i and a_{i+1}). Such a reversible phase transition occurs when the local input arrives at either the voltage threshold or the current threshold of a QD, bringing about size modification of barriers beside it. The cosine envelope of PCQDS response signal is the result of cooperations of oscillated barriers inside PCQDS.

In an arbitrary two-state system, the SR upon dissipative tunneling couples to environment. The SR is caused by the asymmetry of two states of energy. One is the random noise characterized by the asymmetric energy ε_i consisting of periodic perturbation with the frequency ω_s, expressed as $\varepsilon_i(t) = \varepsilon_0 + \delta\varepsilon \times \cos\omega_s t$. Here, ω_s is also the frequency of input noise, known as the source frequency or forcing frequency. The other is the random noise characterized by the temperature T_i and δT, expressed as $T_i(t) = T_0 + \delta T \times \cos\omega_{T_i} t$. The temperature oscillation comes from the phase-change of certain QD.

The peak SNR coincides with the maximum SR can be written as [41]

$$\text{SNR}_i = \frac{\pi}{4} \frac{\Gamma_0}{1 + \exp\left[\dfrac{\varepsilon_i(t)}{k_B T_0}\right]} \left[\delta\left(\frac{\varepsilon_i(t)}{k_B T_i(t)}\right)\right]^2 \tag{1}$$

For different SNR_i, PCQDS has the same ω_s. The PCQDS contains i barriers, namely, i two-state systems, thus we define $\text{SNR} = \prod_1^i \text{SNR}_i / \Gamma_0$. We give $\delta\left[\dfrac{\varepsilon_i(t)}{k_B T_i(t)}\right]_\varepsilon = \dfrac{\delta\varepsilon}{k_B T_0}$ and $\delta\left[\dfrac{\varepsilon_i(t)}{k_B T_i(t)}\right]_T = -\left[\dfrac{\varepsilon_0}{k_B T_0}\right]\dfrac{\delta T}{T_0}$ for the partial perturbations from the force frequency and phase transition oscillation, respectively. For two factors work on the system, we can obtain

$$\text{SNR}(t) = \prod_1^i \frac{\pi}{4} \frac{\Gamma_0}{1 + \exp\left[\dfrac{\varepsilon_0 + \delta\varepsilon \times \cos\omega_s t}{k_B T_0}\right]} \left[\delta\left(\frac{\varepsilon_0 + \delta\varepsilon \times \cos\omega_s t}{k_B (T_0 + \delta T \times \cos\omega_{T_i} t)}\right)\right]^2 \tag{2}$$

Using Eq. (2), we can predict the encoded signals of PCQDSs containing different QDs. Figure 2(c) illustrates the simulation results obtained by using different i values and $\omega_s = 30,000$ Hz, $\omega_{T_{i+1}} = 2\omega_{T_i}$, and $\omega_{T_1} = 3000$ Hz. When $i = 1$, the system does not contain QD because the AlNO layer was undoped, which is proved by the cross-sectional image on high resolution transmission electrical microscopy (HRTEM) (Fig. 2(a)). At this situation, the output spike frequency matches that of the source signal (Fig. 1(a)) and the spike peak does not oscillate with the input history (the first row in Fig. 2(c)). Thus, the simulation matches the experimental fact shown in Fig. 2(b).

The situation of $i = 2$ corresponds to the single QD system, as shown in Fig. 2(d). The output spikes follow the forcing frequency ω_s with the peak values modulated by a cosine envelope (Fig. 2(e)). This response pattern is also replicated in the second row in Fig. 2(c). The situation of $i = 7$ is realized in experiment because six QDs composes a long PCQDS, as shown in Fig. 2(f). The response pattern of PCQDS is plotted in Fig. 2(g). The spike series follow the forcing frequency but its peak envelope exhibits two periodical

Table 1 Comparison of neuronal string and PCQDS spike response signals

	Frequency of spike	Frequency of envelope	Acceleration rate of the spike	Average spikes in a single wave packet
Neuronal string	Equal to the source frequency	1/6 source frequency	$0.24I_0$/period	6
PCQDS	Equal to the source frequency	1/6.5 source frequency	$0.28I_0$/period	6.5

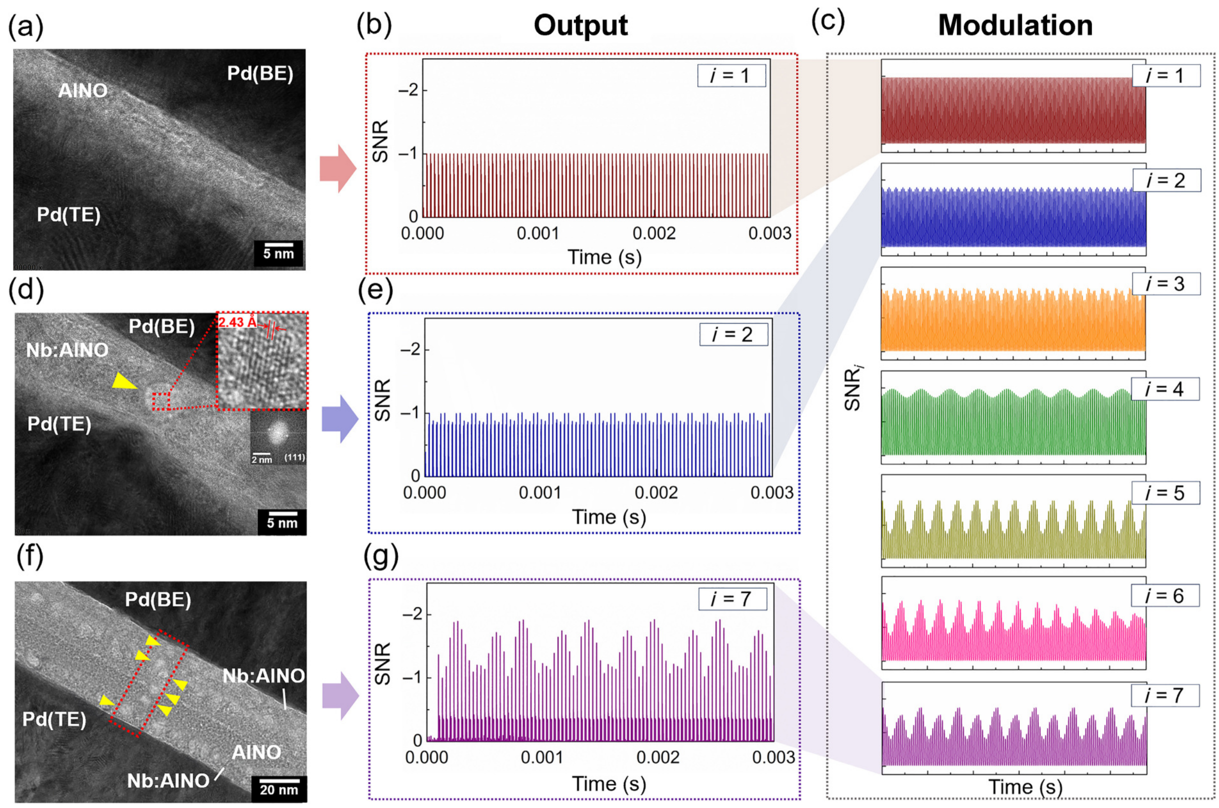

Figure 2 The oscillatory modes for sevral PCQDS systems. (a) Cross-section image under HRTEM for a Pd TE/AlNO/Pd BE device. The system does not contain QD and has only one potential barrier. It is a single two-state structure labelled by $i = 1$. Its signal response is plotted in (b). (c) Simulations of several PCQDSs. The QD number varies from 1 to 6, while the two-state structure increases from $i = 1$ to $i = 7$. (d) HRTEM cross-sectional image and (e) signal response pattern for a single QD system ($i = 2$). (f) HRTEM cross-sectional image and (g) signal response pattern for a PCQDS with six QDs and seven barriers ($i = 7$).

oscillation factors [40]. Obviously, the response pattern in Fig. 2(g) is replicated in the last row in Fig. 2(c). Therefore, the simulation results consistent with the experimental ones demonstrate that our model can reveal the system dynamics in microscopy. We reasonably studied the effects of various inherent non-linearity in a PCQDS by using this SR model. Such a set of simulations will be helpful for us evaluating the possible state of PCQDS when the similar response pattern is obtained in experiment, and also showing how the QDs or neurons couple with each other to generate featured signal patterns.

We firstly designed several situations of inherent non-linearity in a PCQDS, i.e., the oscillation of barriers induced by the phase-change of QD. The QDs are six so that the barriers are seven. We simulated the effects of these situations to signal encoding. If three barriers follow the forcing frequency and the rest oscillate on ω_{T_2}, the ratio ω_{T_2}/ω_s modulates the periodicity of the output envelope significantly, as shown in Fig. 3(a). When the ratio approaches to 0.5, this periodicity is the shortest and the output signal pattern is the most complicated. The ratios near 1 and 0 generate the longest periodicity of the output envelope. This result is also suitable to the other similar situations, in which arbitrary barriers follow the forcing frequency but the rest oscillate on a frequency much lower than the forcing frequency. Figure 3(b) confirms this conjecture. The periodicity of the output envelope is only in the level of several kHz. Figure 3(c) demonstrates a routine to obtain more complicated response pattern. We can set certain QDs to oscillate with forcing frequency at first and set a ratio for the rest QDs in self-oscillation frequencies. For example, we set $\omega_{T_i} = 2\omega_{T_{i-1}} \neq \omega_s$. This establishment give us the featured response patterns in which a short periodical oscillation is embedded in a very long periodical oscillation. The longer periodicity can be 1 to 6 times of the short periodicity.

Figures 4(a) and 4(b) demonstrate that three or more sub-structures of response patterns can appear if the individual barrier can be triggered to oscillate independently. Figure 4(c) shows the details of several typical patterns observed in experiment. The two sets of oscillation can be the same frequency but the oscillation amplitudes can be much different. One weak oscillation pattern can be half of the strong oscillation in the maximum amplitude (the first row in Fig. 4(c)). The two sets can have compatible oscillation amplitudes (the last row in Fig. 4(c)).

We have discovered memory effects in our previous work. The spike peaks oscillated and increased with the input number [22, 23]. We superficially ascribed such a weight modification as synaptic plasticity to the variation of conductive filament. An important reason is that the QDs disperse in the matrix for the Nb-doped AlNO film. We hardly obtain the complete statistic information of the QDs by only using HRTEM technique. However, those response patterns resembling memory or synaptic plasticity appear after we appropriately adjust the individual inherent non-linearity in a PCQDS.

Figures 5(a) and 5(b) show the simulated result after we set a system containing seven barriers. Two barriers oscillate at the frequency of $0.05\omega_s$ and two barriers at $0.1\omega_s$. The rest barriers oscillate at the frequency of $0.03\omega_s$ but have an initial phase difference . The phase difference $= 0$ modulates the peak values to decrease slowly and clearly, indicating forgetting. When we set

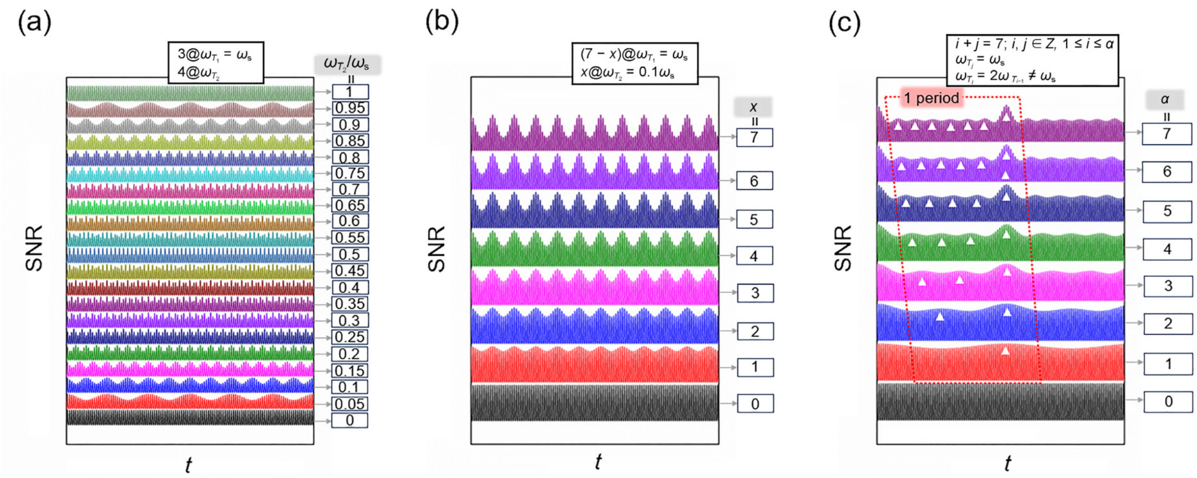

Figure 3 The encoded signal patterns simulated by adjusting the inherent non-linearity in a PCQDS with seven barriers. (a) Three barriers follow the forcing frequency ($\omega_{T_1} = \omega_s$) and four barriers oscillate on ω_{T_2}. The ratio ω_{T_2}/ω_s varies from 1 to 0. (b) x barriers oscillate at the frequency of $0.1\omega_s$, while the rest oscillate at the frequency of ω_s. (c) j barriers oscillate at the frequency of ω_s. For the rest i barriers, the i^{th} barrier oscillates two times of the $(i-1)^{th}$ barrier.

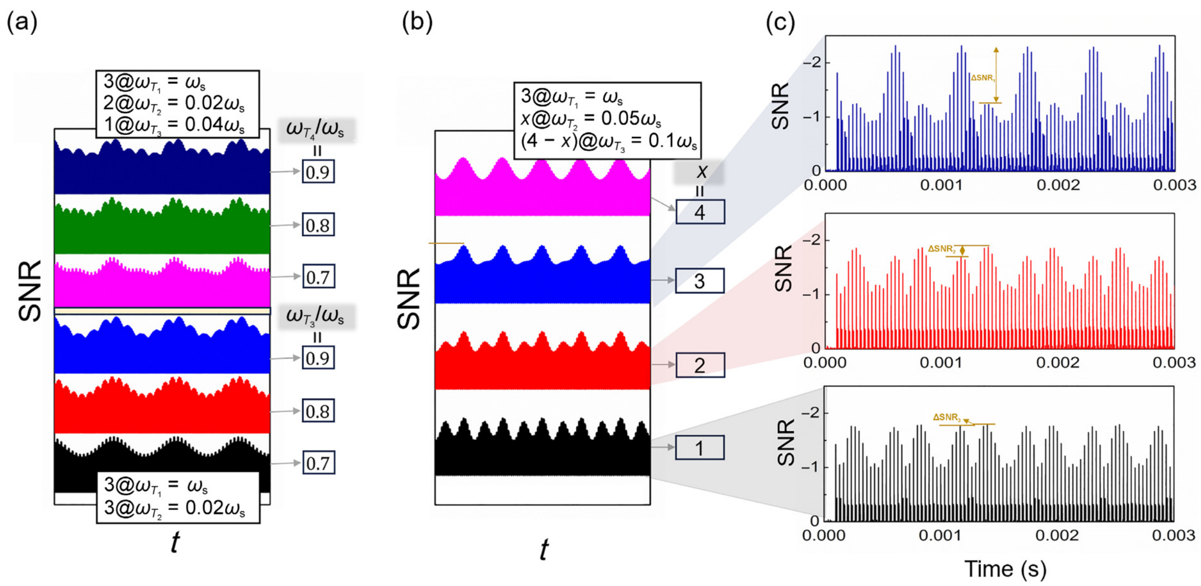

Figure 4 The encoded signal pattern simulated by adjusting the inherent non-linearity in a PCQDS with seven barriers. (a) 3 barriers oscillate at the forcing frequency of ω_s, 2 barriers at $0.02\omega_s$ and the rest at $0.04\omega_s$. (b) 3 barriers oscillate at the forcing frequency of ω_s, x barriers at $0.05\omega_s$, and $4-x$ barriers at $0.1\omega_s$. The local details in (b) are enlarged in (c).

$= \frac{\pi}{4}$, we got that the peak values increase gradually, suggesting memory formation. When we set $\frac{\omega_{T_3}}{\omega_s} = 1$ and $= 0$, we obtained that the peak values do not change after long term stimulation, indicating that neither memory nor forgetting occurs. In addition, the ratio $\frac{\omega_{T_3}}{\omega_s}$ can modulate the peak values significantly in a small range (shown in Fig. 5(c)), indicating SRDP.

We understood memory in certain new scope according to above results. First, the system only composed of volatile elementary unit is able to generate memory effect. The string connecting several PCQDs has this function. Thus, the memory may exist in system or network. The QDs oscillate independently in particular frequency. The self-oscillating frequencies and the phases are mutually different. This situation may result in charges lagging or oscillating among the QDs. The consequence is the generation of memory or forgetting. We may need to establish more elaborate model to handle the charge oscillation between QDs. Second, the variation time in Fig. 5(b) may be very long to let us observe LTP or long-term memory. Third, the memory or forgetting condition may be different for the particular signal or signal pattern. Therefore, rousing memory needs the same signal pattern or its segment.

Finally, we tried to recover the responses in Fig 1(c) according to our model. We kept up with the input width and height but modulated the oscillation parameters of the barriers, i.e., enhanced ω_s to 36,000, and adopted $\omega_{T_1} = 3000$ while $\omega_{T_i} = 100$ for the other barriers. We have successfully obtained the oscillation patterns in Fig. 6, greatly resembling output waveform in Fig. 1(c). Therefore, it is feasible to make the signal response of the PCQDS more closely resemble that of native healthy mouse myocardial fibers.

Comparing with the previous work [40], we extended the model to the categories of 1 to 7 barriers, i.e., a two-state system to seven two-state systems in this work. The simulations prove the generalization of the theory of PCQDS. We also found that the

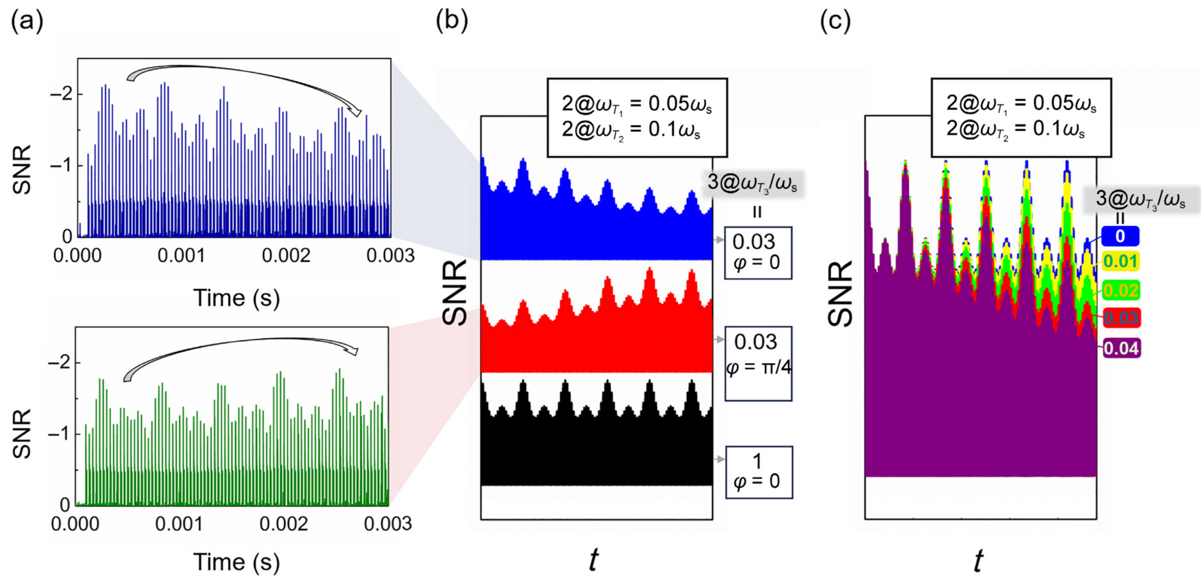

Figure 5 Memory effects simulated by modulating phase difference. Memory patterns: (a) The average peak value during an oscillation period decreases with the time suggesting forgetting, while that increases with time suggesting memory. (b) Simulation results: 2 barriers oscillate at the frequency of $0.05\omega_s$ and 2 barriers at $0.1\omega_s$. 3 barriers oscillate at the frequency of $0.03\omega_s$. The oscillations are influenced by a phase difference of . (c) 2 barriers oscillate at the frequency of $0.05\omega_s$ and 2 barriers at $0.1\omega_s$. 3 barriers oscillate at the frequencies of 0 to $0.04\omega_s$ and $= 0$.

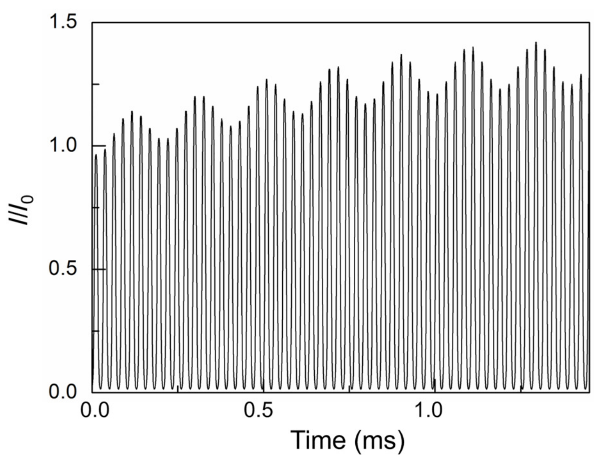

Figure 6 The simulation of the responses of cardiac and arterial tissue to structured signals.

previous work focused on the staged data around 5000 or 10,000 times but neglected some interesting results. The detailed analysis in this work found that some results involved in the learning and forgetting processes. We can validate certain biological observation by modulating oscillation parameters. These all strengthen our understanding in encoding signal and memory when the information flows in the neural network.

Therefore, the above model can describe or predict the possible output wave patterns responded by either a neural string or a PCQDS. Certainly, we will consider more complicated situations beyond the assumptions established in simulations. For instance, the size of QDs and the distance between them are assumed even. This will vary if the input energies of either individual pulse or signal series change suddenly and seriously. The interest is to find whether this mutation would result in long term modification, which cannot be recovered. We also wonder whether the statistic distribution of QDs should be introduced and the influence of environmental temperature, etc.

Current biological technologies can detect the degree and extent of actions in different cortexes when an event occurs. Our study proposes a research method to infer the relationship between these actions and signal outputs or decisions and to gradually establish physical framework. In addition, the widely interested pulsed neural networks (spiking neural network (SNN)) provide a biorealistic approach in which neurons enhance noisy signals through SR, which requires the system to be non-linear. Therefore, introducing the inherent nonlinearity of nanoscale into the hardware to prepare a stochastic resonance device to simulate artificial neurons can improve the response ability of neurons to weak signals, thus reducing the power consumption of transmitted information and enhancing the processing ability of the device. The PCQDS may become as a platform to explore artificial neuron. Our model may provide a theoretical basis for simulating SNN and neuromorphic computation of complex QD systems.

3 Conclusions

We successfully constructed the PCQDS systems and studied their signal responses by an SR model. The PCQDS is actually a cascaded structure consisted of several SR two-state system that the signal responses can be modulated by inherent non-linearity, i.e., the phase-change of QDs. According to simulation we know that some QDs will oscillate with the input forcing frequency, while certain QDs will oscillate in their own frequency due to phase transition. These two effects cooperate to generate polymorphic response patterns, including action potential exhibited by the envelope of response spikes peaks. An interesting and important simulation is that we replicate the memory effect in Nb-doped AlNO, i.e., a QDs dispersed system. The result indicates that memory can occur in a system only constructed by volatile elementary units, implying memory existing in network. LTP and SRDP can also be realized by modulating self-oscillation frequency and phase difference. Our study provides a new scope to study signal handling in quantum system and memory effect.

4 Experimental

Pd BE and TE were prepared by using magnetron sputtering. Nb-doped AlNO was prepared by using co-sputtering. Electrical characterizations were performed using an Agilent B1500A semiconductor parameter analyzer with a B1530 waveform function generator. Electrical measurements were performed on the probe platform in a glove box filled with nitrogen to avoid contaminations from oxygen, water, and carbon dioxide. The low-temperature threshold switching behavior was measured using a low-temperature and high-magnetic electronic transport measurement platform (CRYOGENIC, CRYOGENIC4084) and a direct-current power source (Keysight B2901A). A compliance current of 1 μA was applied to avoid a hard breakdown of the devices. The cross-sectional profile of the device was analyzed using HRTEM (JEM-2100F). The Nb content in AlNO film was controlled by the number of Nb slices embedded in the AlNO target, while the concentration and size of quantum dots were controlled by the voltage amplitude loaded on the device.

The transmission electron microscopy (TEM) samples were fabricated using a focused ion beam (FIB). The atomic images were studied using a fast Fourier transform (FFT).

Data availability

All data needed to support the conclusions in the paper are presented in the manuscript. Additional data related to this paper may be requested from the corresponding author upon request.

Acknowledgments

The study was supported by the National Natural Science Foundation of China (No. 51972192).

Declaration of competing interest

All the contributing authors report no conflict of interests in this work.

Author contribution statement

Q. W. fulfilled materials preparation, device fabrication, electric measurement, structure characterization and paper writing. F. Z. designed the experiments and wrote the paper. Z. A. L. and J. W. Y. assisted in electric measurement. F. P. discussed the results and the paper. All the authors have approved the final manuscript.

Use of AI statement

None.

References

[1] Gammaitoni, L.; Hänggi, P.; Jung, P.; Marchesoni, F. Stochastic resonance. *Rev. Mod. Phys.* **1998**, *70*, 223–287.

[2] McDonnell, M. D.; Abbott, D. What is stochastic resonance. Definitions, misconceptions, debates, and its relevance to biology. *PLoS Comput. Biol.* **2009**, *5*, e1000348.

[3] Stein, M. B.; Roy-Byrne, P. P.; Craske, M. G.; Bystritsky, A.; Sullivan, G.; Pyne, J. M.; Katon, W.; Sherbourne, C. D. Functional impact and health utility of anxiety disorders in primary care outpatients. *Med. Care.* **2005**, *43*, 1164–1170.

[4] Ma, W. J.; Beck, J. M.; Latham, P. E.; Pouget, A. Bayesian inference with probabilistic population codes. *Nat. Neurosci.* **2006**, *9*, 1432–1438.

[5] Sumner, L. W.; Mendes, P.; Dixon, R. A. Plant metabolomics: Large-scale phytochemistry in the functional genomics era. *Phytochemistry* **2003**, *62*, 817–836.

[6] Mold, J. W.; Vesely, S. K.; Keyl, B. A.; Schenk, J. B.; Roberts, M. The prevalence, predictors, and consequences of peripheral sensory neuropathy in older patients. *J. Am. Board Fam. Pract.* **2004**, *17*, 309–318.

[7] Faisal, A. A.; Selen, L. P. J.; Wolpert, D. M. Noise in the nervous system. *Nat. Rev. Neurosci.* **2008**, *9*, 292–303.

[8] Bahar, S.; Moss, F. Stochastic resonance and synchronization in the crayfish caudal photoreceptor. *Math. Biosci.* **2004**, *188*, 81–97.

[9] Jaramillo, F.; Wiesenfeld, K. Mechanoelectrical transduction assisted by Brownian motion: A role for noise in the auditory system. *Nat. Neurosci.* **1998**, *1*, 384–388.

[10] Chatterjee, M.; Robert, M. E. Noise enhances modulation sensitivity in cochlear implant listeners: Stochastic resonance in a prosthetic sensory system. *J. Assoc. Res. Oto.* **2001**, *2*, 159–171.

[11] Douglass, J. K.; Wilkens, L.; Pantazelou, E.; Moss, F. Noise enhancement of information transfer in crayfish mechanoreceptors by stochastic resonance. *Nature* **1993**, *365*, 337–340.

[12] Collins, J. J.; Imhoff, T. T.; Grigg, P. Noise-enhanced information transmission in rat SA1 cutaneous mechanoreceptors via aperiodic stochastic resonance. *J. Neurophysiol.* **1996**, *76*, 642–645.

[13] Ivey, C.; Apkarian, A. V.; Chialvo, D. R. Noise-induced tuning curve changes in mechanoreceptors. *J. Neurophysiol.* **1998**, *79*, 1879–1890.

[14] Mendez-Balbuena, I.; Manjarrez, E.; Schulte-Mönting, J.; Huethe, F.; Tapia, J. A.; Hepp-Reymond, M. C.; Kristeva, R. Improved sensorimotor performance via stochastic resonance. *J. Neurosci.* **2012**, *32*, 12612–12618.

[15] Fallon, J. B.; Carr, R. W.; Morgan, D. L. Stochastic resonance in muscle receptors. *J. Neurophysiol.* **2004**, *91*, 2429–2436.

[16] Peña-Romo, A.; Ríos-Rodríguez, A.; Escalante-Acosta, B.; Rodríguez-González, J. Presence of stochastic resonance in isolated mouse heart. In *Proceedings of the World Congress on Medical Physics and Biomedical Engineering 2018*, Prague, Czech Republic, 2019, pp 889–895.

[17] Martínez, L.; Pérez, T.; Mirasso, C. R.; Manjarrez, E. Stochastic resonance in the motor system: Effects of noise on the monosynaptic reflex pathway of the cat spinal cord. *J. Neurophysiol.* **2007**, *97*, 4007–4016.

[18] Hareland, K. J. M. Impact of vibration and stochastic resonance electrical stimulation on muscle contraction. Master Degree Thesis, Oklahoma State University, Stillwater, OK, USA, 2021.

[19] Cek, M. E.; Uludag, I. F. Spectral resonance in Fitzhugh-Nagumo neuron system: Relation with stochastic resonance and its role in EMG signal characterization. *Cogn. Neurodyn.* **2024**, *18*, 1779–1787.

[20] Kurita, Y.; Shinohara, M.; Ueda, J. Wearable sensorimotor enhancer for fingertip based on stochastic resonance effect. In *Proceedings of 2011 IEEE International Conference on Robotics and Automation*, Shanghai, China, 2013, pp 3790–3795.

[21] Perc, M.; Gosak, M. Pacemaker-driven stochastic resonance on diffusive and complex networks of bistable oscillators. *New J. Phys.* **2008**, *10*, 053008.

[22] Wan, Q.; Zeng, F.; Yin, J.; Sun, Y. M.; Hu, Y. D.; Liu, J. L.; Wang, Y. C.; Li, G. Q.; Guo, D.; Pan, F. Phase-change nano-clusters embedded memristor for simulating synaptic learning. *Nanoscale* **2019**, *11*, 5684–5692.

[23] Wan, Q.; Zeng, F.; Sun, Y. M.; Chen, T. J.; Yu, J. W.; Wu, H. Q.; Zhao, Z.; Cao, J. L.; Pan, F. Memristive behaviors dominated by reversible nucleation dynamics of phase-change nanoclusters. *Small* **2022**, *18*, 2105070.

[24] Wan, Q.; Zeng, F.; Yu, J. W.; Chen, T. J.; Lu, Z. A.; Pan, F. Local activity in a self-assembled quantum dot system. *Adv. Quantum Technol.* **2023**, *6*, 2300021.

[25] Peters, K. J. H.; Geng, Z.; Malmir, K.; Smith, J. M.; Rodriguez, S. R. K. Extremely broadband stochastic resonance of light and enhanced energy harvesting enabled by memory effects in the nonlinear response. *Phys. Rev. Lett.* **2021**, *126*, 213901.

[26] Jennings, C.; Ma, X. Y.; Wickramasinghe, T.; Doty, M.; Scheibner, M.; Stinaff, E.; Ware, M. Self-assembled InAs/GaAs coupled quantum dots for photonic quantum technologies. *Adv. Quantum Technol.* **2020**, *3*, 1900085.

[27] Merrill, D. R.; Bikson, M.; Jefferys, J. G. R. Electrical stimulation of excitable tissue: Design of efficacious and safe protocols. *J. Neurosci. Methods* **2005**, *141*, 171–198.

[28] Kaye, A. D.; Ridgell, S.; Alpaugh, E. S.; Mouhaffel, A.; Kaye, A. J.; Cornett, E. M.; Chami, A. A.; Shah, R.; Dixon, B. M.; Viswanath, O. et al. Peripheral nerve stimulation: A review of techniques and clinical efficacy. *Pain Ther.* **2021**, *10*, 961–972.

[29] Sdrulla, A. D.; Guan, Y.; Raja, S. N. Spinal cord stimulation: Clinical efficacy and potential mechanisms. *Pain Pract.* **2018**, *18*, 1048–1067.

[30] Krauss, J. K.; Lipsman, N.; Aziz, T.; Boutet, A.; Brown, P.; Chang, J. W.; Davidson, B.; Grill, W. M.; Hariz, M. I.; Horn, A. et al. Technology of deep brain stimulation: Current status and future directions. *Nat. Rev. Neurol.* **2021**, *17*, 75–87.

[31] Hänggi, P.; Jung, P.; Zerbe, C.; Moss, F. Can colored noise improve stochastic resonance. *J. Stat. Phys.* **1993**, *70*, 25–47.

[32] Benzi, R.; Sutera, A.; Vulpiani, A. The mechanism of stochastic resonance. *J. Phys. A: Math. Gen.* **1981**, *14*, L453.

[33] Collins, J.; Chow, C. C.; Capela, A. C.; Imhoff, T. T. Aperiodic stochastic resonance. *Phys. Rev. E* **1996**, *54*, 5575.

[34] Longtin, A. Stochastic resonance in neuron models. *J. Stat. Phys.* **1993**, *70*, 309–327.

[35] Wellens, T.; Shatokhin, V.; Buchleitner, A. Stochastic resonance. *Rev. Mod. Phys.* **2003**, *67*, 45.

[36] Lindner, B.; García-Ojalvo, J.; Neiman, A.; Schimansky-Geier, L. Effects of noise in excitable systems. *Phy. Rep.* **2004**, *392*, 321–424.

[37] Wu, Y. C.; Feng, J. W. Development and application of artificial neural network. *Wirel. Pers. Commun.* **2018**, *102*, 1645–1656.

[38] Katz, A. M. *Physiology of the Heart*, 5th ed.; Lippincott Williams & Wilkins: Philadelphia, 2011.

[39] Haddock, R. E.; Hill, C. E. Rhythmicity in arterial smooth muscle. *J. Physiol.* **2005**, *566*, 645–656.

[40] Wan, Q.; Zeng, F.; Lu, Z. A.; Yu, J. W.; Chen, T. J.; Pan, F. Adaptive signal modulation evolved by the inherent nonlinearity of phase-change quantum-dot string. *Nano Lett.* **2024**, *24*, 8089–8097.

[41] Löfstedt, R.; Coppersmith, S. N. Quantum stochastic resonance. *Phys. Rev. Lett.* **1994**, *72*, 1947–1950.